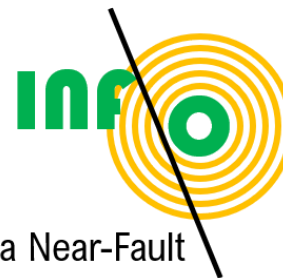


Seismic sequence Rocca San Felice 04-06/07/2020

Gaetano Festa, Guido Maria Adinolfi, Francesco Carotenuto, Alessandro Caruso, Simona Colombelli, Grazia De Landro, Luca Elia, Antonio Emolo, Sergio Gammaldi, Antonio G. Iaccarino, Antonio Iorio, Sahar Nazeri, Rosario Riccio, Guido Russo, Antonio Scala, Matteo Picozzi and Aldo Zollo



Università degli studi
di Napoli Federico II



Irpinia Near-Fault
Observatory



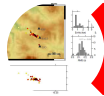
Summary



Data



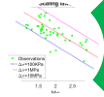
Seismotectonic setting



Location and Refined Catalog



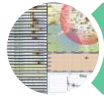
Focal mechanisms



Source Parameters

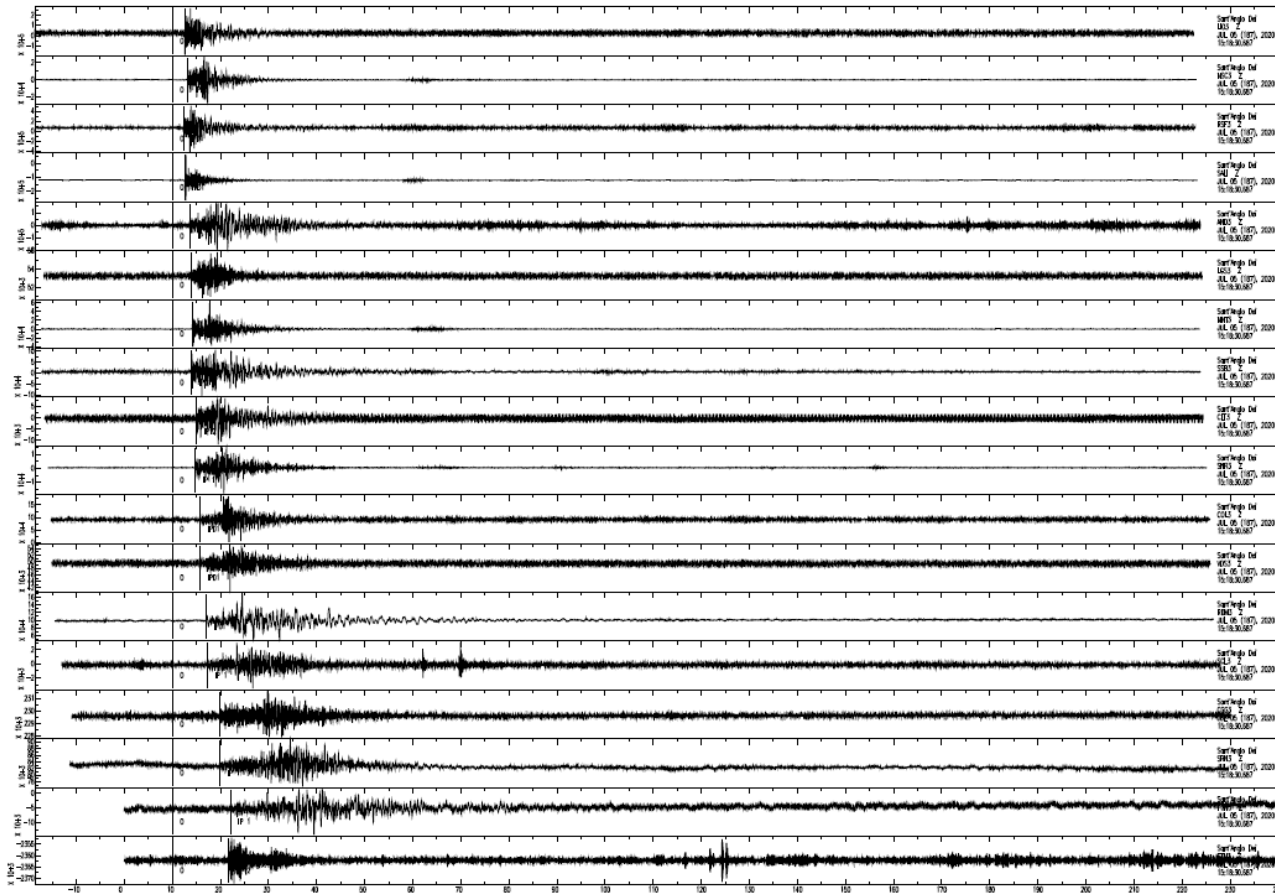


Ground motion



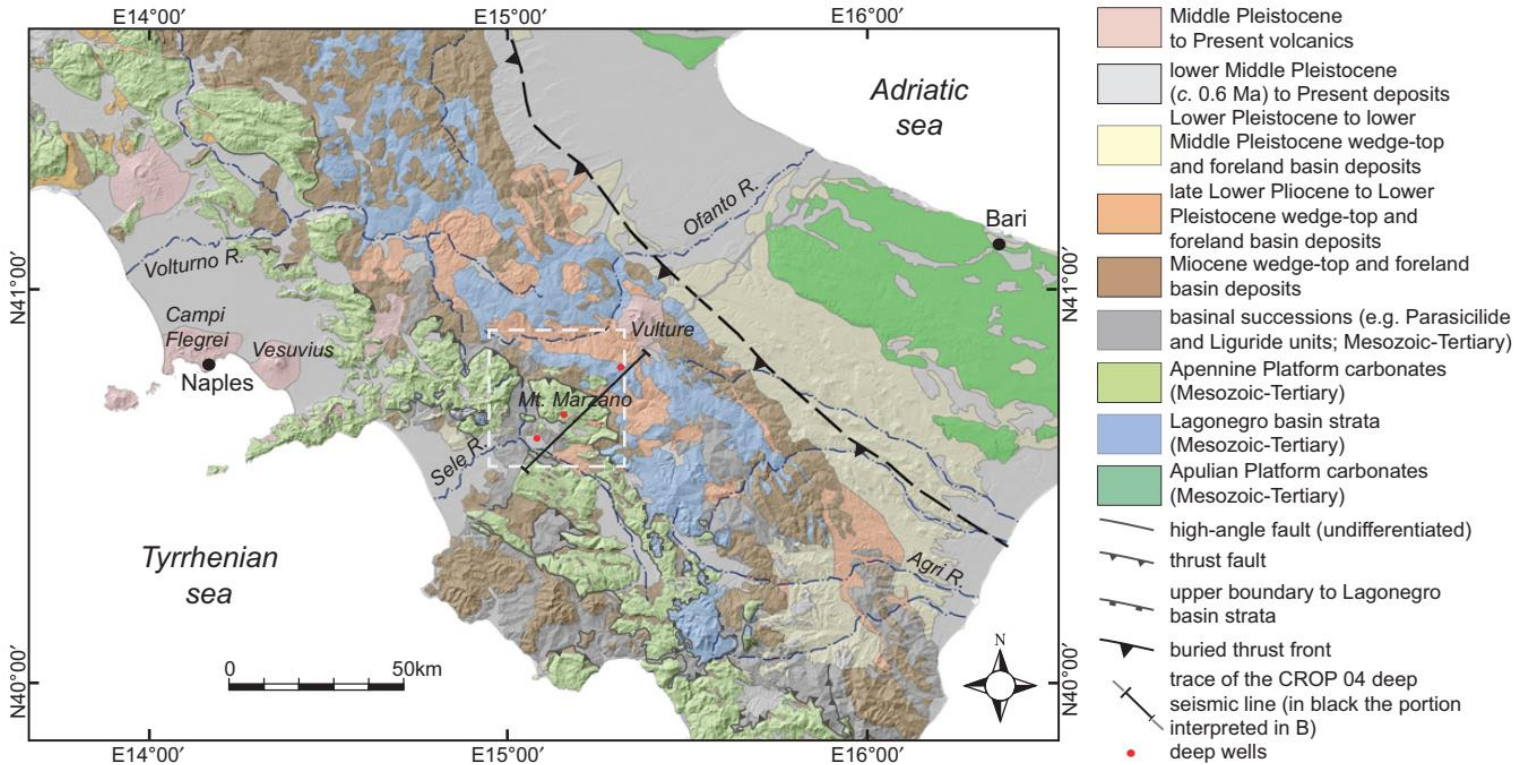
Earthquake Early Warning

Seismic records at ISNet



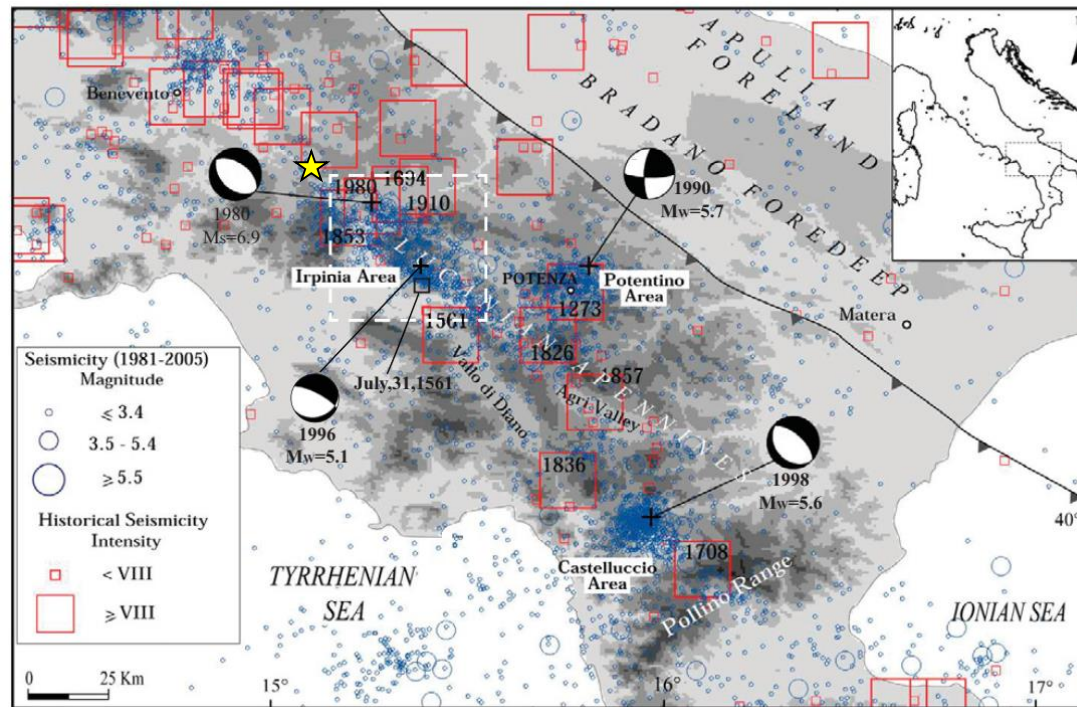
Here you see an example of **seismic waveforms (vertical component)** recorded at the stations of ISNet, for the event of M2.7, (5/7/2020-15:18) in the distance range **3-70 km**. Even at the farthest stations the waveforms show a **large signal to noise ratio**.

Geological Setting



The sequence occurred along the Southern Apennines chain, a fold and thrust belt characterized by ENE-verging duplexes geometries and out-of-sequence thrusting due to orogenic contraction. It has been active since upper Eocene-Oligocene Miocene till late Pliocene. During the Quaternary the Southern Apennines thrust belt was dissected by NW-SE oriented normal faults that accommodated an **extensional tectonic phase**, according to a stress field with the axis of maximum extension coaxial to the axis of maximum compression of Apennines belt (Doglioni 1995; Patacca et Scandone, 2007a, Ascione, 2013). The figure shows the geological sketch map of Southern Apennines derived from Ascione et al. (2013).

Historical and Instrumental Seismicity



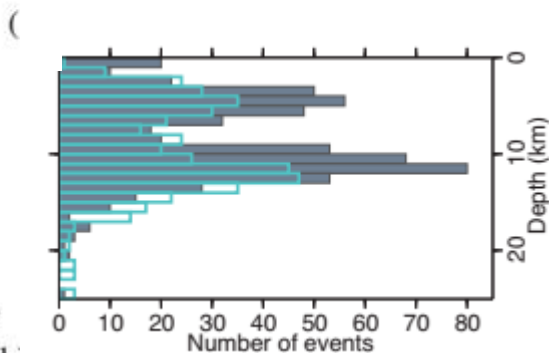
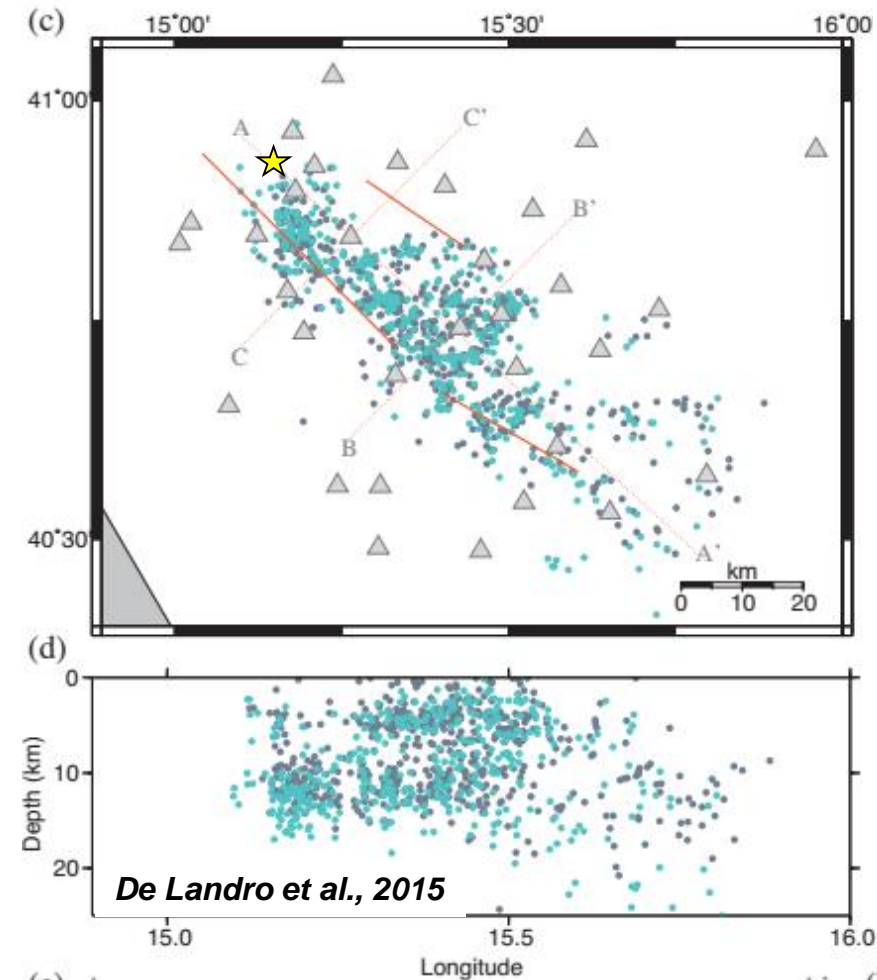
Several historical earthquakes struck the Irpinia region with MCS intensity $I \geq X$, occurred in A.D. 989, 1694, 1930, and 1962 (*CPTI Working Group, 2019; Ascione et al., 2013*). **The Ms 6.9, 1980 Irpinia earthquake** was the most destructive, instrumental earthquake of Southern Apennines **occurred along a system of NW-SE trending normal faults**. This event is described by a complex rupture process involving multiple fault segments according to (at least) three different nucleation episodes at 0 s, 20 s and 40 s times (e.g. *Bernard and Zollo, 1989*). In 1996 a seismic sequence with a mainshock of Mw 5.1 took place (*Cocco et al., 1999*) inside the epicentral area of 1980 earthquake. In the figure the (historical and instrumental) seismicity and the focal mechanisms of the main last decade earthquakes are reported. The location of the Rocca San Felice seismic sequence is indicated by the yellow star.

Instrumental Seismicity

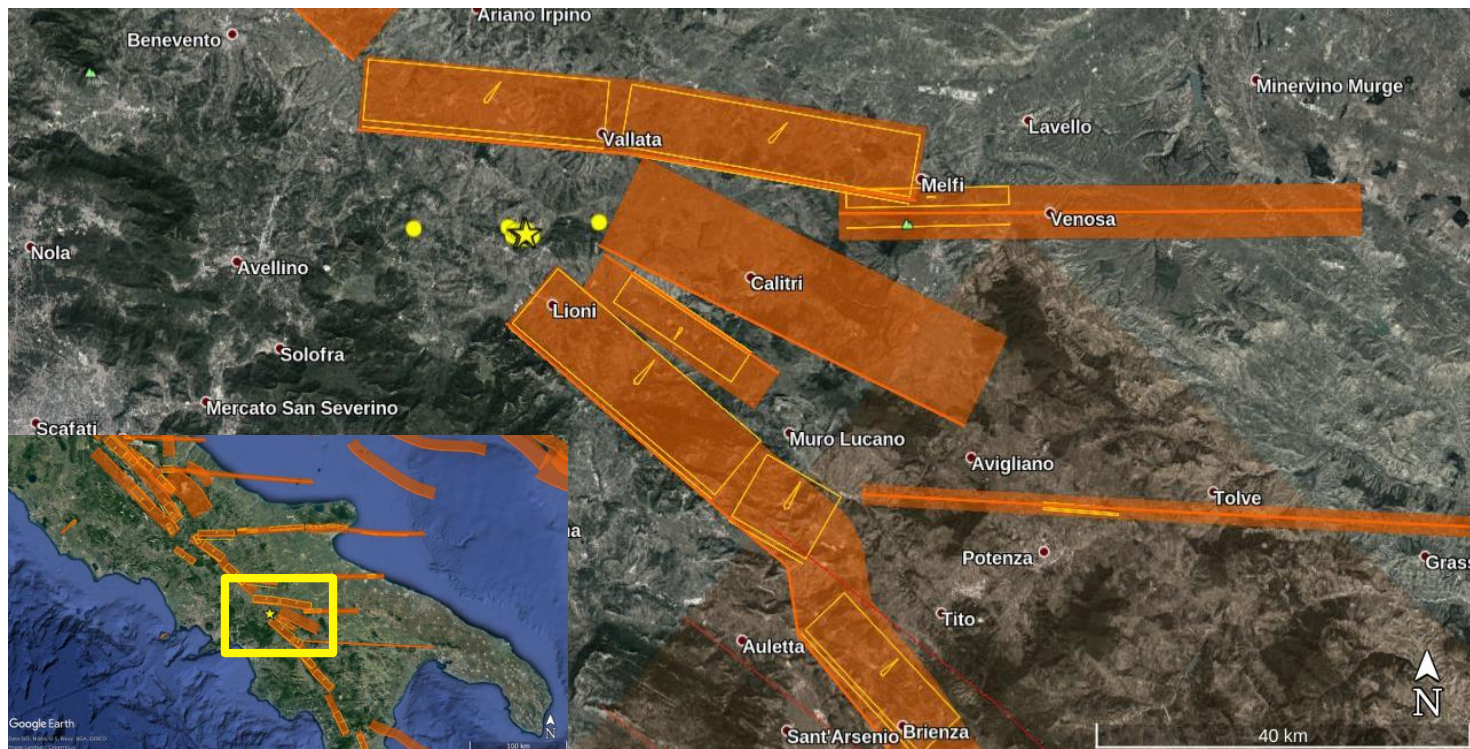
The present-day low-magnitude seismicity ($ML < 3.3$) occurs mainly in the upper 15 km of the crust and shows fault plane solutions varying between **pure-normal** and **normal-strike** kinematics according to a dominant SW–NE extensional regime (De Matteis et al., 2012; De Landro et al., 2015; Ascione et al., 2013, Adinolfi et al., 2019).

The background low magnitude seismicity and the related stress field are **closely linked** with the major fault segments activated during the **1980 Irpinia earthquake**.

In the figure the double-difference earthquake locations of seismicity from 2005 August to 2011 April (manually revised data in grey, cross-correlated revised in turquoise) are reported. Red lines are the surface projection of the three fault segments that ruptured during the 1980 Irpinia earthquake. The location of the Rocca San Felice seismic sequence is indicated by the yellow star.

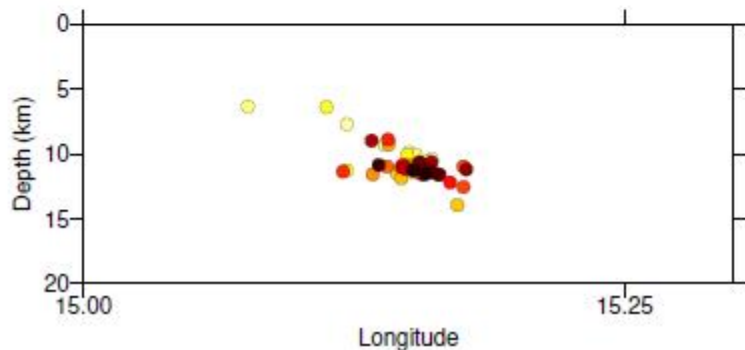
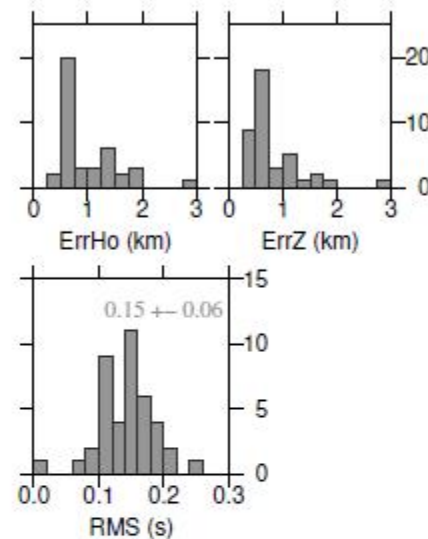
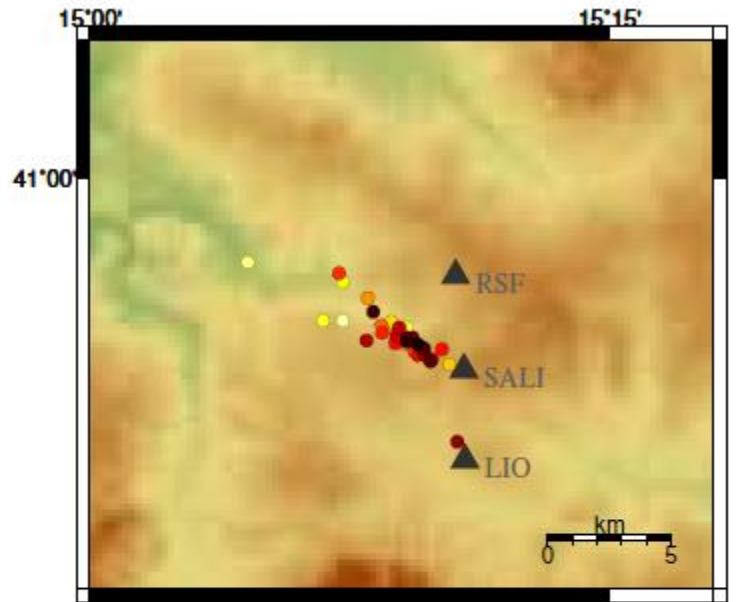


Seismotectonic Context



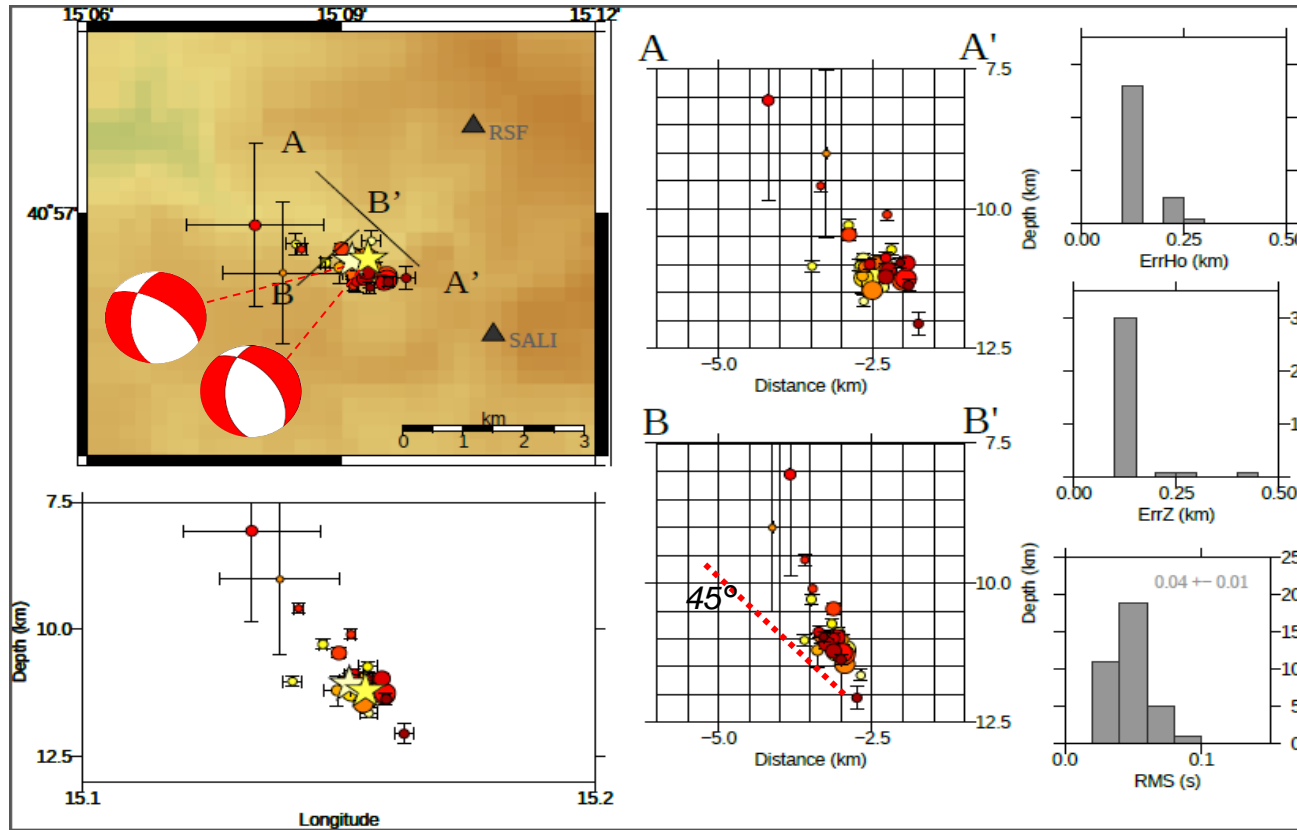
Historical earthquakes up to X-XI MCS intensities and instrumental seismicity with moderate to large events depict the Southern Apennines as a region with one of the **highest seismic hazard** of the Mediterranean area, with segmented, seismogenic structures (lateral extent of few tens of kilometers) capable of **generating up to M 7 earthquakes** (Chiarabba et al, 2005; Improta et al., 2014). Rocca San Felice seismic sequence occurred near the northern tip of the NE-dipping fault segment activated during the **Ms 6.9, 1980 Irpinia earthquake**. In the figure the sources of earthquakes larger than ML 5.5 in Southern Apennines are reported (DISS Working Group, 2018). The location of the seismic sequence is indicated by yellow circles and stars.

3D Absolute locations



The absolute locations of 43 automatically detected events have been computed using the software **NLLoc** (Lomax *et al.*, 2009). The inversion is performed in the **3D velocity model** for the area (Amoroso *et al.*, 2014); P and S picks are manually measured. The color scale in the Figure corresponds to the time occurrence of the events (from yellow-time=0 to red-time=2days). The resulting location shows events distributed along the NW-SE direction, over a narrow zone 4-5 km long. The location errors are within 1 km and RMS residuals within 0.2 s for most of the events.

3D Double-Difference locations (1/2)



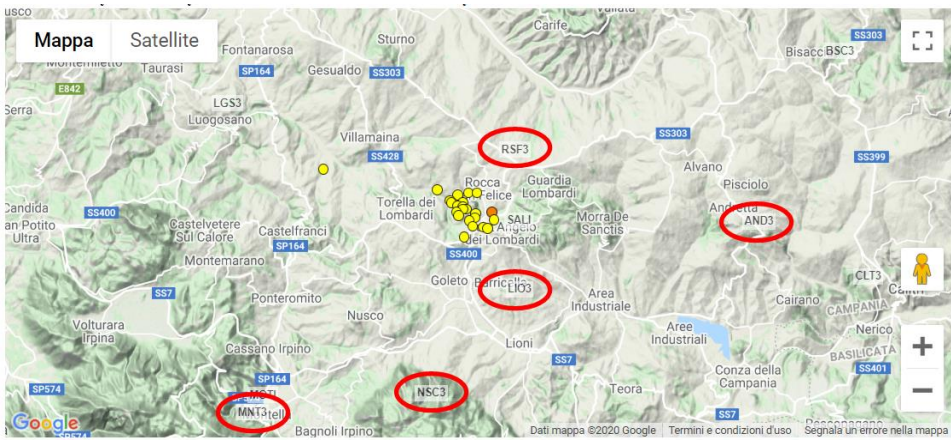
For this further refined analysis, **36 events** have been selected, based on a threshold on the minimum number of picks and the quality of the absolute locations. The **double-difference locations** are obtained with the software **NLDiffLoc** (De Landro et al., 2015), in the 3D velocity model for the area (Amoroso et al., 2014), using the same manual picks. After relative relocation, events appear more clustered in space and they **clearly identify a NW-SE faulting zone** (extent; 1.5 km along-strike, 2 km along-dip) having an approximate **dip of 45°** (see sect BB')

3D Double-Difference locations (2/2)

Main hints from the refined event location

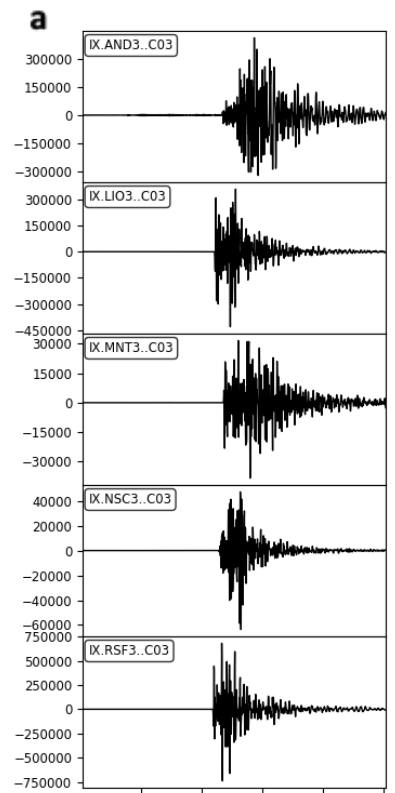
- Events are clustered with an extension of the pattern **covering a size of 2-3 km** and an alignment in **the NW-SE** direction.
- Event depths are between **10 km and 12.5 km**. In section, the events clearly delineate a fault plane with a dip **of about 45°** and NE immersion.
- This result is **consistent with the focal mechanisms** of the two largest events and enables for plane selection (see slide 19 and following).
- Location errors are within **few hundred meters** for most of the events and **rms are within 0.1 s**

FAST catalog (1/2)



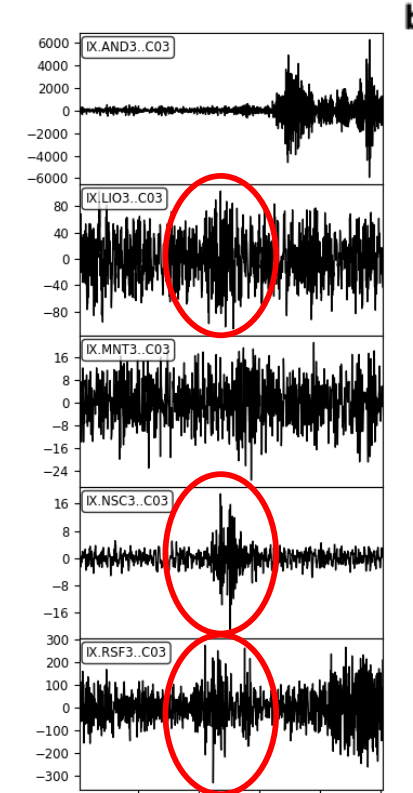
The automatic system of the network detected 43 events. We explored the **continuous helicorder** through the autocorrelation algorithm **FAST** (Yoon *et al.*, 2015, Bergen & Beroza 2018) to improve the detection of microearthquakes. We used the vertical component of the velocimeters at **5 stations with a distance ranging from about 3 km to 17 km** from the sequence centroid. We retrieved **342 events** detected at least at 2 stations with a local magnitude ranging from **0.0 to 3.0**. On the right the waveforms for the main event (panel a - M 3.0 07/03 16:14:25) and for an event of M 0.0 (panel b MI=0.0 07/03 20:37:00).

2020-07-03T16:14:06.395453 - 2020-07-03T16:14:56.408449



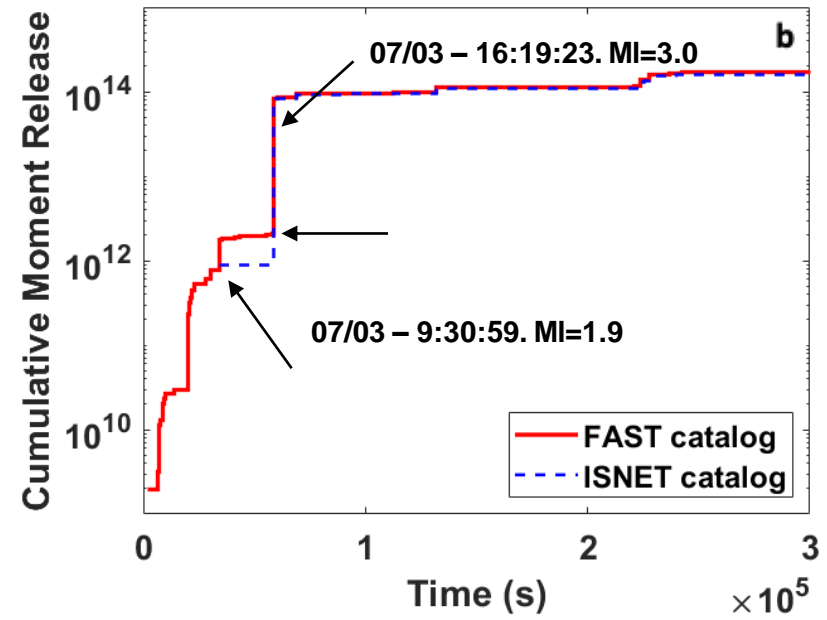
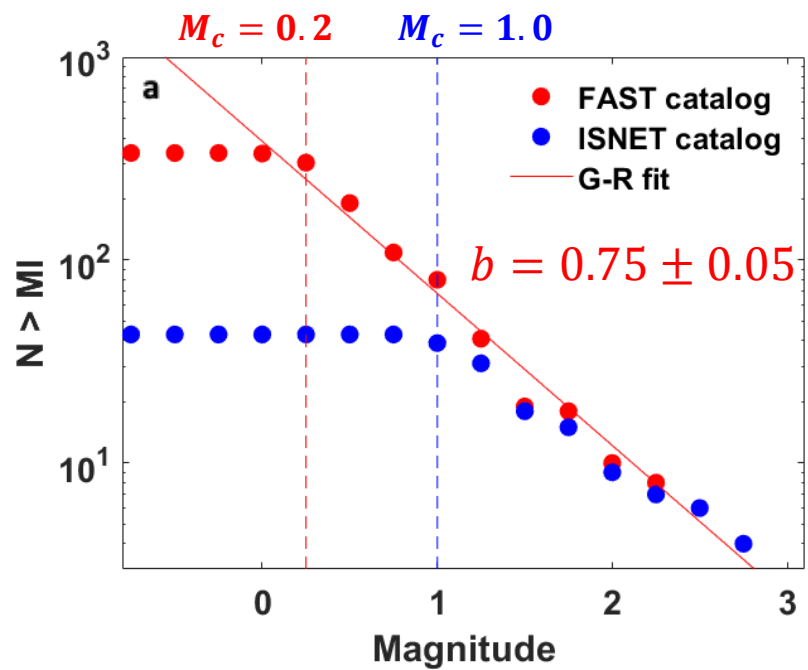
Main event – M=3.0
Declared at 5 stations

2020-07-03T20:36:50.396656 - 2020-07-03T20:37:40.409652



Event MI=0.0
Declared at 3 stations

FAST catalog (2/2)



We investigated the **magnitude-frequency distribution** for the refined catalog, comparing it with the ISNET automatic catalog (panel a). We estimated a **magnitude of completeness of 0.2**, almost 1 unit smaller than the value from the automatic detections (1.0). We also reported the **b-value estimate of $b=0.75 \pm 0.05$** . This is significantly larger than the value inferable from the automatically detected events (0.57 ± 0.03). The latter estimate cannot be considered a robust estimate due to the scarcity of events. **The cumulative seismic moment release** (panel b) is not significantly different for the two catalogs yielding an equivalent **total magnitude of M 3.5**. However, we can recognize a sequence of events preceding the two largest (ML 3) events in the sequence, started about **14 hours before** the first event detected by the automatic procedures of ISNet (MI=1.9 – 23 events).

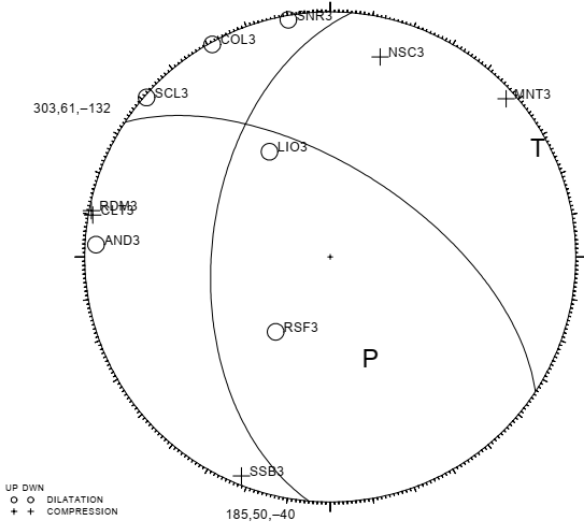
Focal Mechanisms

20200703 16:14 25.54 (MULTIPLE) RMS = 0.18 S ERH = 0.6 KM
 40 56.25 15 9.01 DMIN = 3 KM ERZ = 0.7 KM
 DEPTH = 9.62 KM AZM GAP = 154 MISFIT = 0.09 (+.05)
 MAG = 0.00 # FM = 11 STD R = 0.62

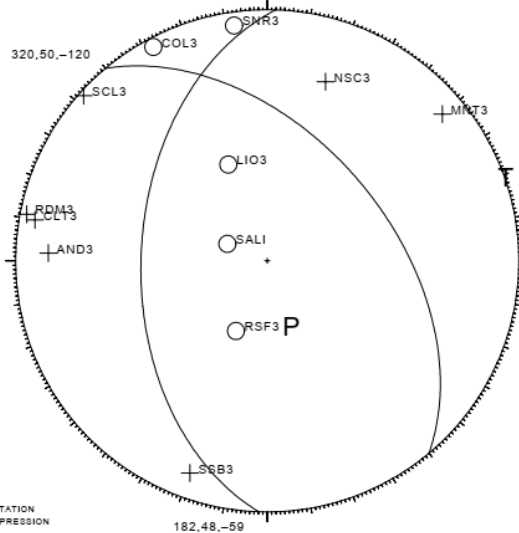
STRIKE UNCERTAINTY = 8
 DIP UNCERTAINTY = 10
 RAKE UNCERTAINTY = 0
 % MACHINE PICKS = 0

20200703 16:19 23.63 (MULTIPLE) RMS = 0.15 S ERH = 0.5 KM
 40 56.21 15 9.57 DMIN = 1 KM ERZ = 0.7 KM
 DEPTH = 10.55 KM AZM GAP = 150 MISFIT = 0.00 (+.05)
 MAG = 0.00 # FM = 12 STD R = 0.63

STRIKE UNCERTAINTY = 8
 DIP UNCERTAINTY = 8
 RAKE UNCERTAINTY = 10
 % MACHINE PICKS = 0



DISCREPANT OBSERVATIONS
 STAT DIST AZM AIN PRMK
 AND3 15 93 95 1905

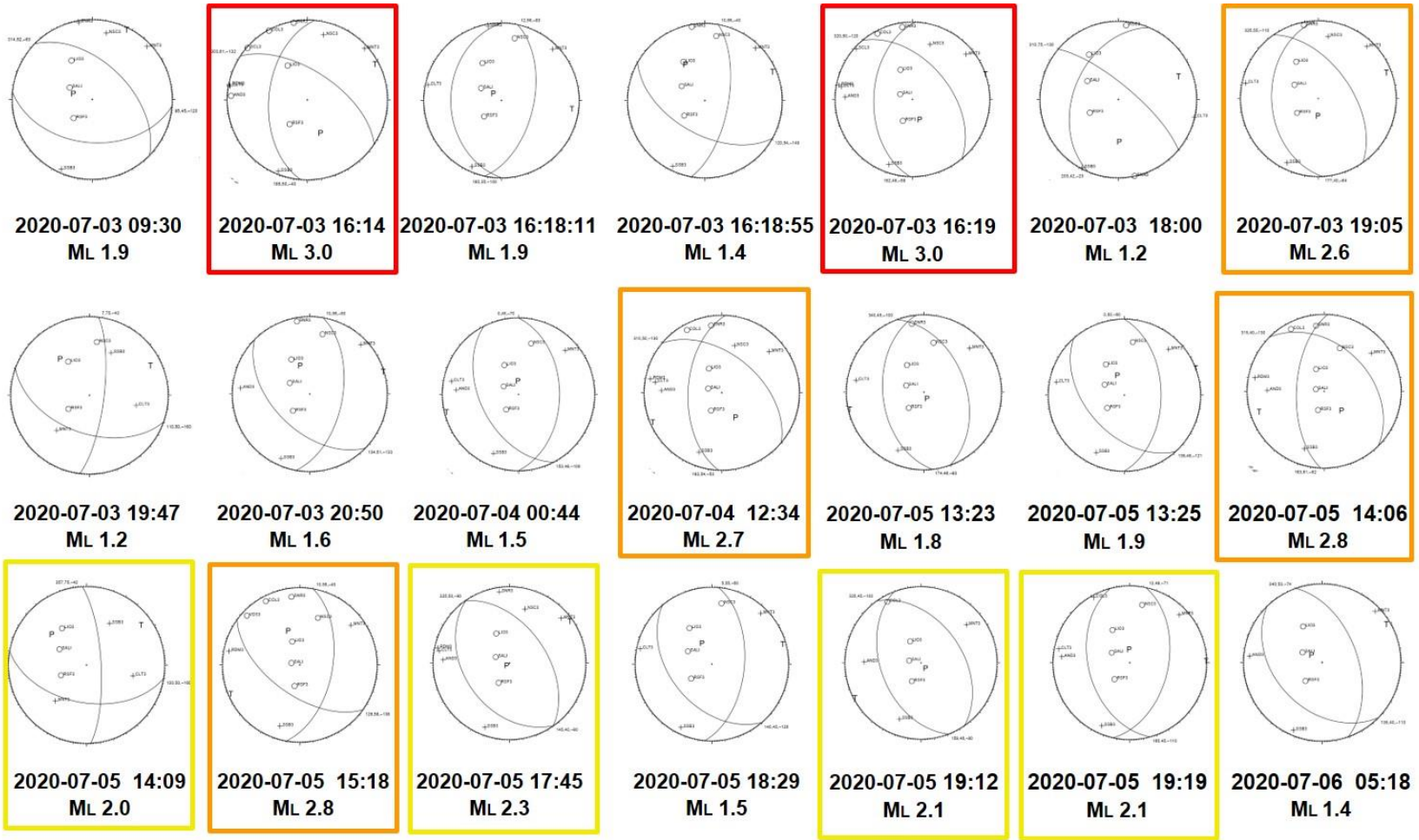


2020-07-03 16:14
ML 3.0

2020-07-03 16:19
ML 3.0

We computed the focal mechanism solutions from inversion of **P-wave polarities** using the FPFIT code (*Rosenberg and Oppenheimer, 1985*). The solutions for the two main earthquakes of the sequence are shown in the Figure. The solutions show a similar **normal-fault kinematics** with a minor strike-slip component. The entire set of solutions is shown in the following slide.

Focal Mechanism Catalog

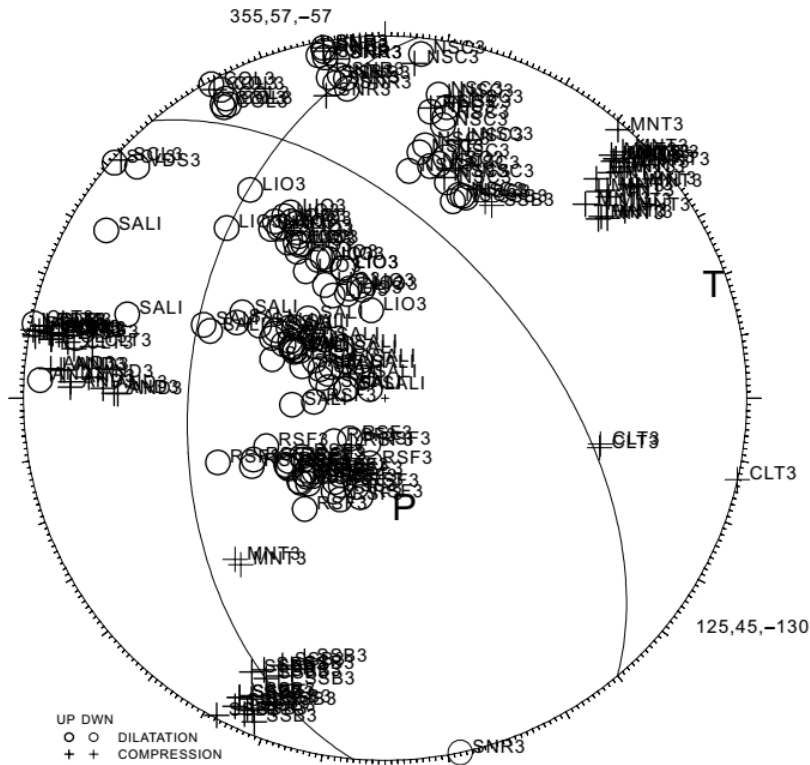


ML = 3.0

2.5 < ML < 3.0

2.0 < ML < 2.5

Composite Focal Mechanisms



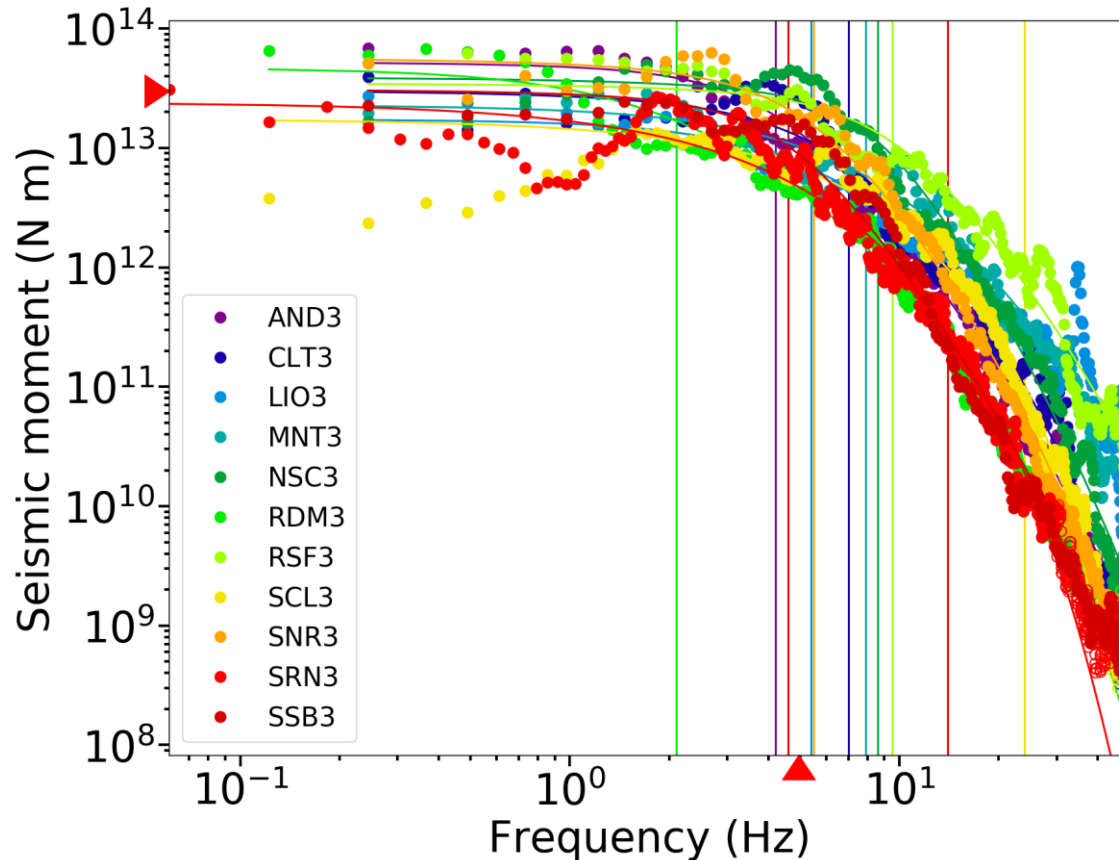
<i>Station</i>	<i>Polar.</i>	<i>No.</i>	<i>Polar.</i>	<i>No.</i>
AND3	UP	9	DOWN	1
CLT3	UP	16	DOWN	1
COL3	UP	1	DOWN	6
LIO3	UP	0	DOWN	30
MNT3	UP	27	DOWN	0
NSC3	UP	8	DOWN	18
RDM3	UP	6	DOWN	0
RSF3	UP	1	DOWN	33
SALI	UP	0	DOWN	38
SCL3	UP	1	DOWN	1
SNR3	UP	4	DOWN	11
SSB3	UP	22	DOWN	0
VDS3	UP	0	DOWN	1

We finally computed a **composite focal mechanism** solution from the inversion of P-wave polarities for the two main earthquakes of the sequence. On the same focal sphere, we represent all the **available 235 polarities**. We see that some stations show a change in the polarity along the sequence: these stations are near the focal planes and constrain the mechanism.

Focal Mechanisms - Summary

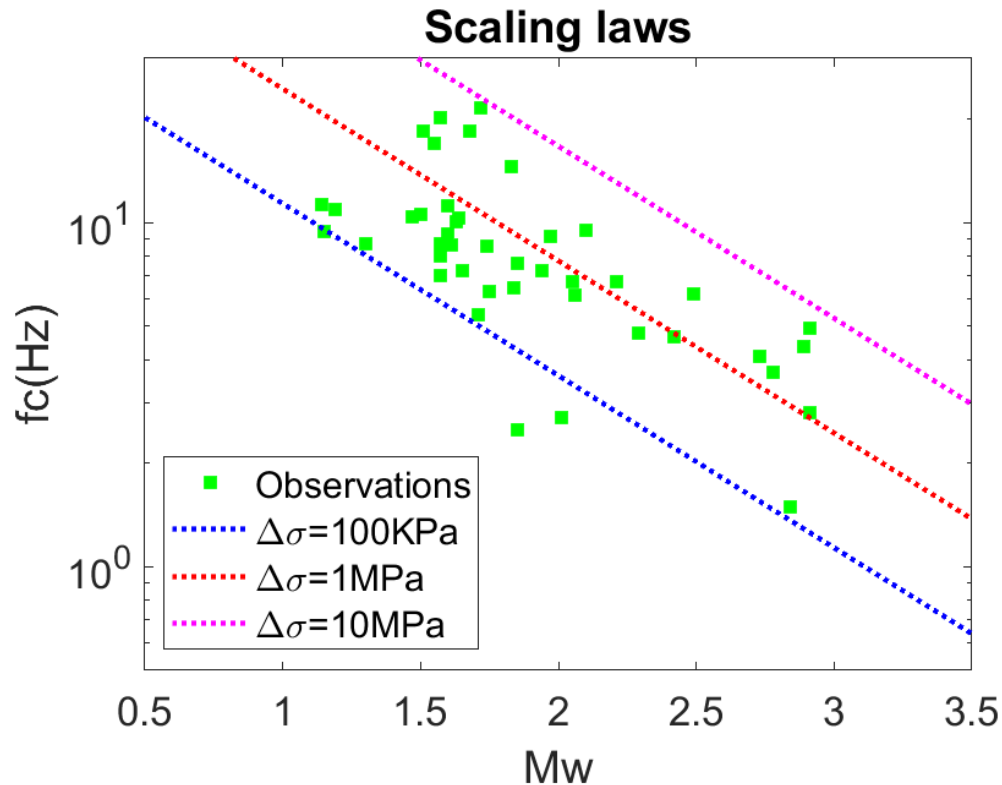
- **21 fault plane solutions** are computed from the inversion of P-wave polarities for earthquakes with magnitude ranging between 1.2 and 3.0.
- Fault plane solutions show **normal fault kinematics** with a minor, variable strike-slip component. Despite the uncertainty of the solutions due to the small number of available data and the small size of the events, a good agreement between the solutions can be noted.
- A large group of seismic stations show the same P-wave polarity highlighting a similar rupture kinematics and fault plane geometry during the evolution of seismic sequence.
- Focal mechanism solutions of the main earthquakes show the activation of a **NW-SE striking** fault structure **with 50°-60° dip**, in a good agreement with seismogenic sources of the Irpinia region.
- Considering the earthquake locations of the seismic sequence, **the NE-dipping nodal plane can be considered as the preferential plane** along which the seismic sequence originated. In fact, its geometry is in good agreement with spatial hypocentre distribution.

Source Parameters – SPAR (1/3)



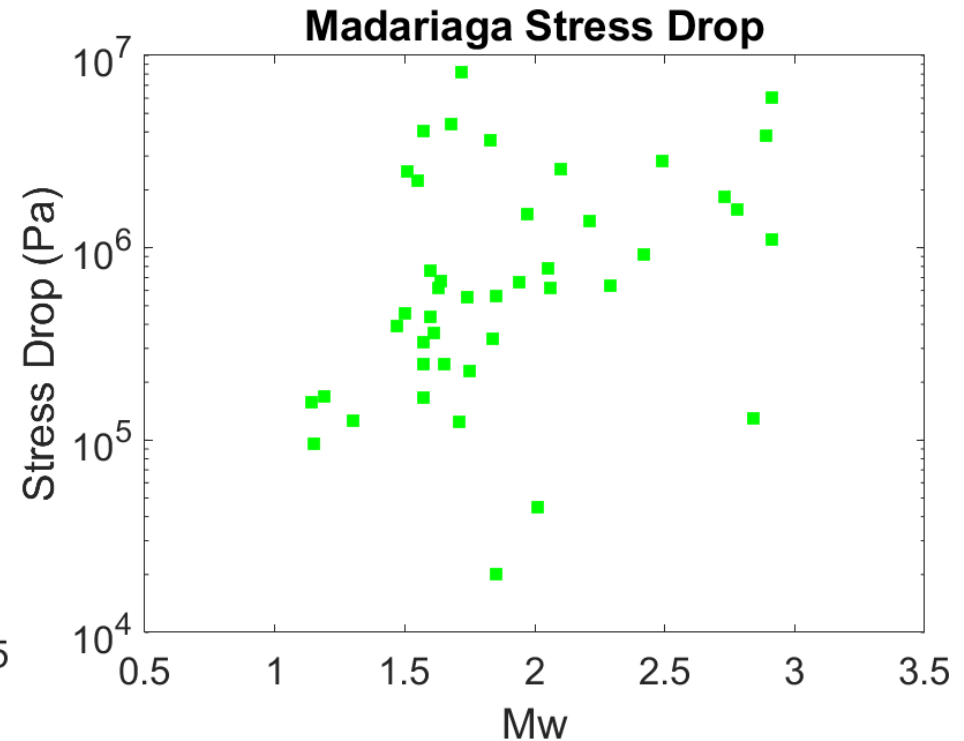
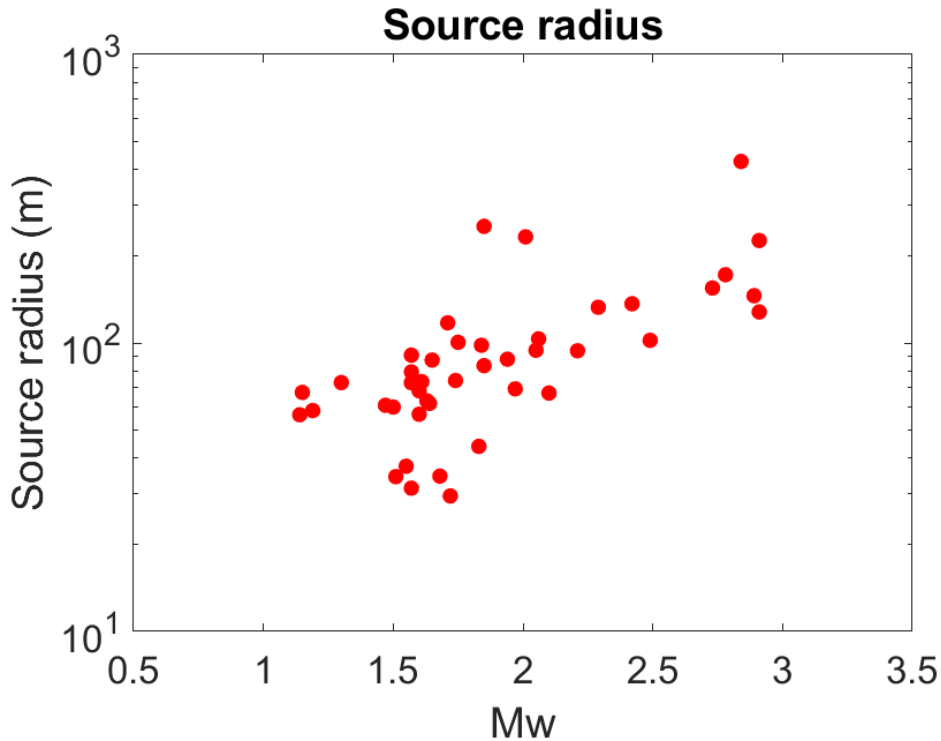
Source parameters have been computed for the 43 events of the sequence, automatically detected by the ISNet management system. **Displacement amplitude spectra** from observations have been modelled using a generalized Brune source model, through the software **SPAR** (Supino et al., 2019). For the event in the Figure we estimated an average moment magnitude of $M_w=2.91 \pm 0.02$, a corner frequency of $f_c=5.0 \pm 0.2$ Hz and a spectral fall-off of $\gamma=2.42 \pm 0.04$.

Source Parameters – SPAR (2/3)



The corner frequency vs M_w plot shows that the **self-similarity can be assumed for the sequence**, with an average stress drop of **0.64 MPa**. The stress drop has been computed using the circular rupture model of Madariaga. For the main events in the sequence, the stress drop is larger: we found **an average stress drop of 1.0 MPa** for events with magnitude $M > 2$. For small magnitude events, the estimation of the corner frequency can be affected by the limited bandwidth and the anelastic attenuation effect.

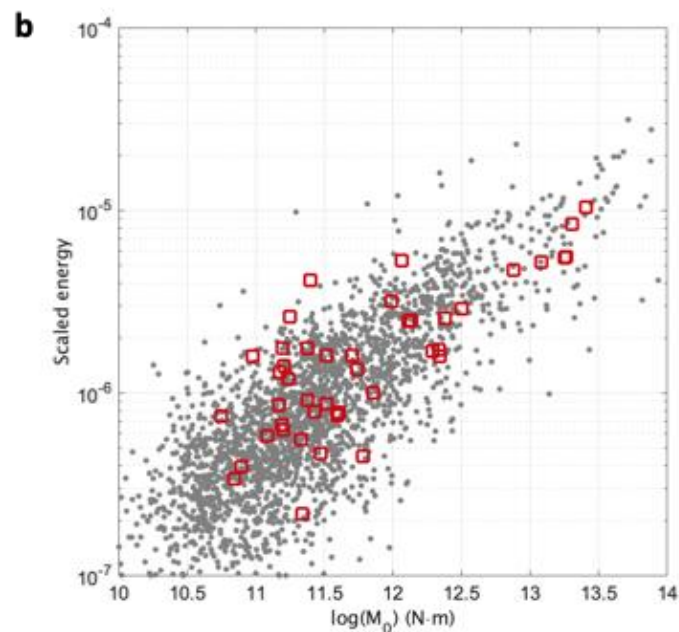
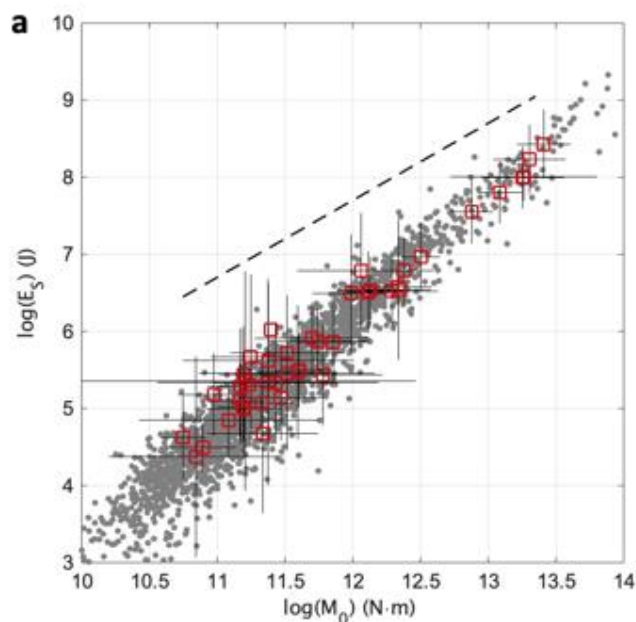
Source Parameters – SPAR (3/3)



We found that the source radius ranges from **150-400 m** for the largest magnitude events in the sequence and between **30-60 m for a M1.5 events**. The stress drop plot in the right panel shows scattered points (over about two orders of magnitude) , with no specific trend with moment magnitude.

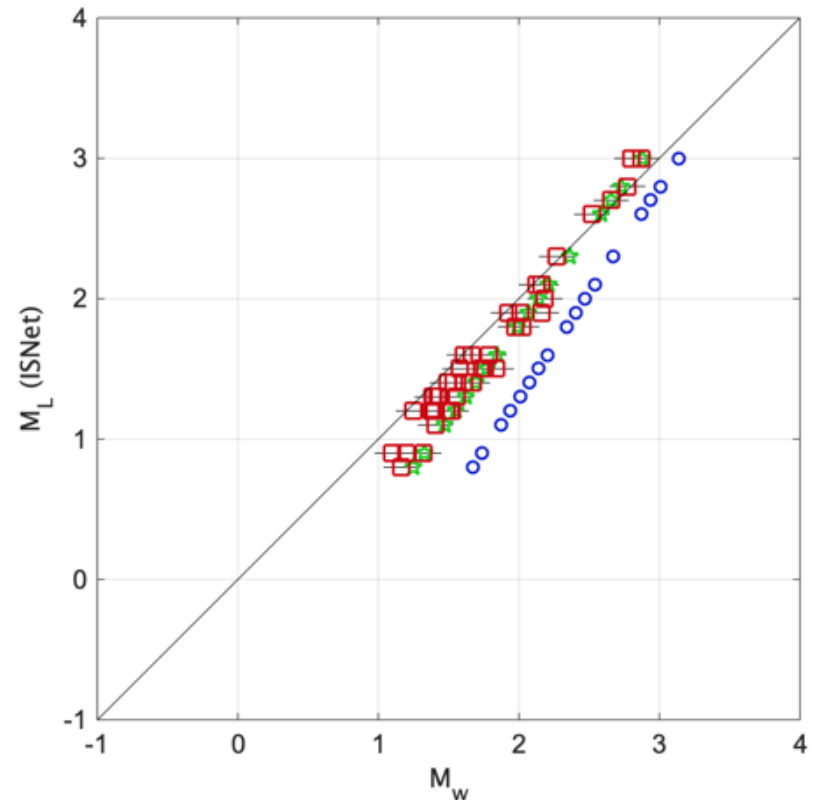
Source Parameters – TimeFit (1/2)

We have also estimated M_0 and E_S from the S-wave time windows applying the procedure in the time domain proposed by *Picozzi et al. (2018)* and (2019). **The energy-to-moment scaling** observed for the sequence is in good agreement with values estimated for the Irpinia seismicity. Figure (a) shows that the seismicity of the present sequence exhibits **smaller stress-drop** than that assumed by Kanamori as global average (from 2 to 6 MPa, dashed line): the diverse slope here suggests a possible deviation from self-similar behavior. Also the scaled energy increases as a function of the M_0 (Figure b).



Source Parameters – TimeFit (2/2)

We finally computed the **moment magnitude** (M_w) for the earthquakes of the sequence and compared these estimates with the **local magnitude** (M_L) from ISNet bulletin. As shown in the Figure to the side, the M_L - M_w scaling is linear but does not follow a 1:1 line. If we compute theoretical M_w values from M_L using a model calibrated by *Malignini and Munafò (2018)*, for Italy (blue dots), we observe a deviation from experimental data. On the contrary, these latter are in very good agreement with theoretical values obtained starting from M_L , and using the relation calibrated by *Bobbio et al. (2009)* for the Irpinia region. These results suggest that M_0 estimates are robust. Also the moment magnitude **shows a +0.2 shift** with respect to the local magnitude at small magnitudes ($1 < M < 2$)

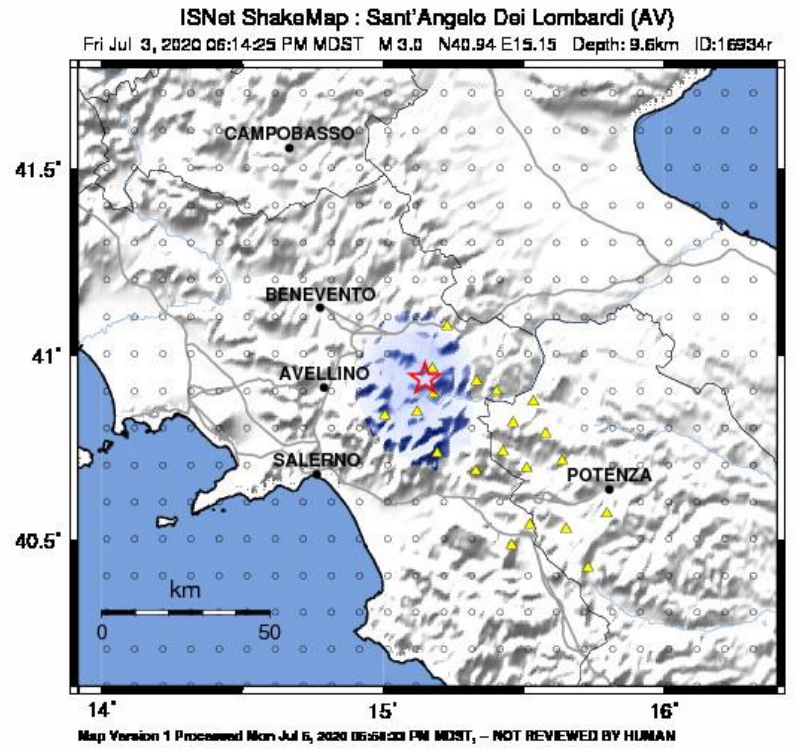
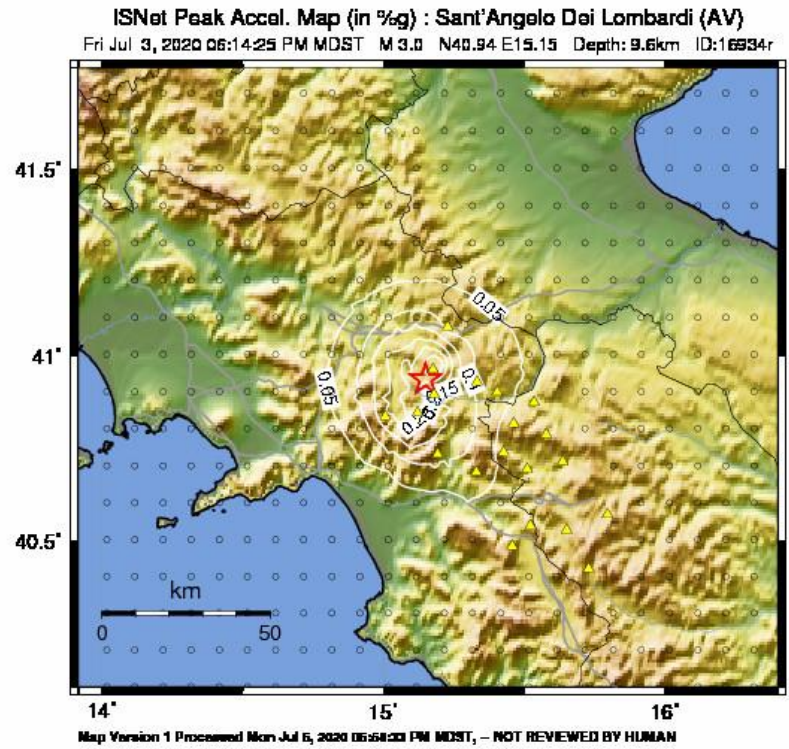


Source Parameters

Hints from source parameters

- Events show corner frequencies that scale with seismic moment. For $M > 2$ the scaling is consistent with self-similarity and an average stress drop of **1.0 MPa**. **When including all the events, the average stress drop is 0.64 MPa.**
- Source radius ranges between **30-60m for a M1.5** event and **150-400 m for a M 3** event.
- **Radiated energy increases with seismic moment** at a faster rate than global average estimates, and **at lower dynamic stress drops.**
- **Moment magnitude** of the events is consistent with **local magnitude**, with a **0.2 shift** at small magnitudes.

PGA-Intensity – ShakeMap – M3.0 3/7/20 – 16:14

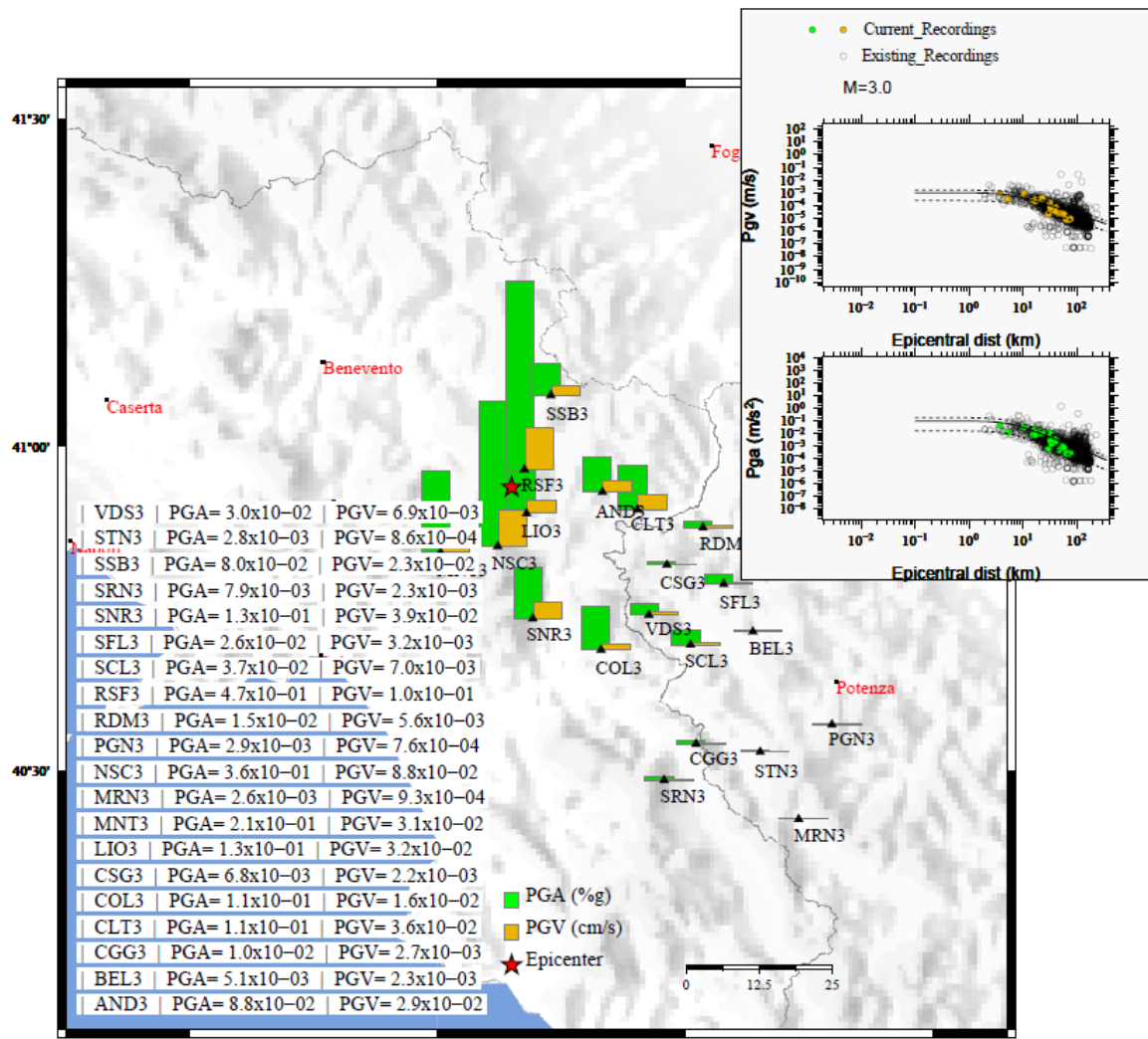


Here we represent the PGA and Intensity maps computed with ShakeMap software for the M3.0 event (3/7/2020 at 16.14). The plots show maps slightly elongated along the NS direction, indicating a source/path effect

PERCEIVED SHAKING	Not felt	Weak	Light	Moderate	Strong	Very strong	Severe	Violent	Extreme
POTENTIAL DAMAGE	none	none	none	Very light	Light	Moderate	Moderately/Heavy	Heavy	Very Heavy
PEAK ACC. (%g)	<0.17	0.17-0.4	0.4-0.8	0.8-1.2	1.2-1.8	1.8-3.4	3.4-8.5	8.5-12.4	>12.4
PEAK VEL. (cm/s)	<0.1	0.1-1.1	1.1-3.4	3.4-8.1	8.1-18	18-31	31-80	80-118	>118
INSTRUMENTAL INTENSITY	I	II-III	IV	V	VI	VII	VIII	IX	X+

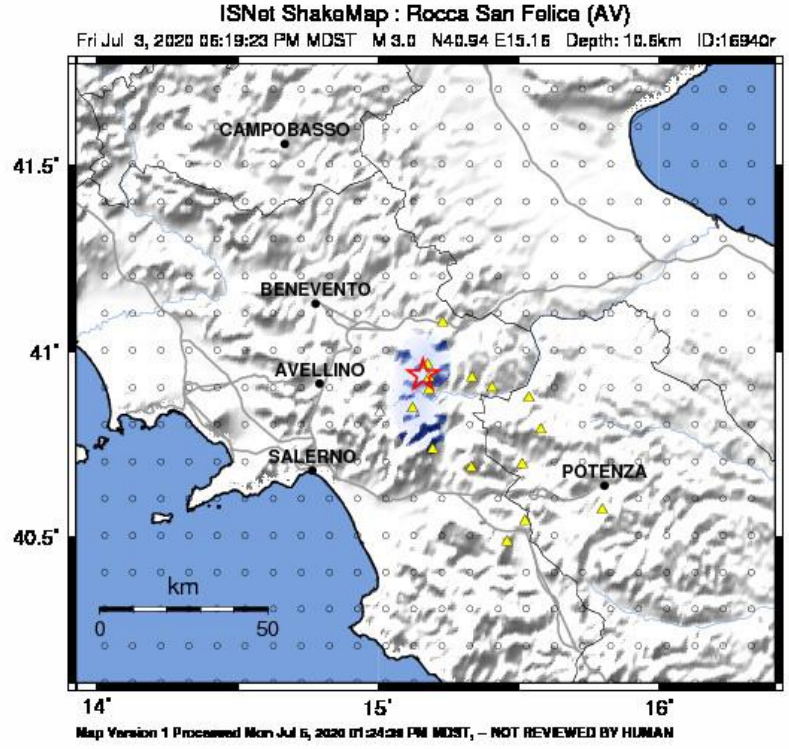
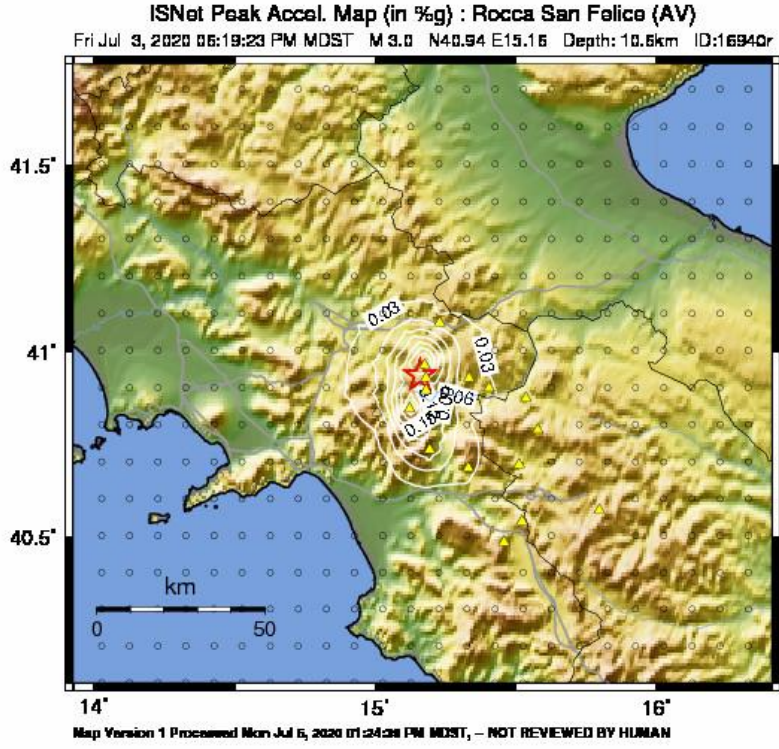
GMPE - M3.0

3/7/20 - 16:14



When we represent the peak amplitudes (**PGA and PGV**) for the stations, we observe maximum peak amplitudes for stations nearby the epicenter. Along the Apennine direction, south of the epicentre, the peak amplitudes are larger than in the Anti-Apennine direction. On average **peak amplitudes match the GMPEs** retrieved for the area (*Emolo et al., 2011*). However, PGV values show a faster decrease with amplitude, likely owing to larger attenuation.

PGA-Intensity – ShakeMap – M3.0 3/7/20 – 16:19

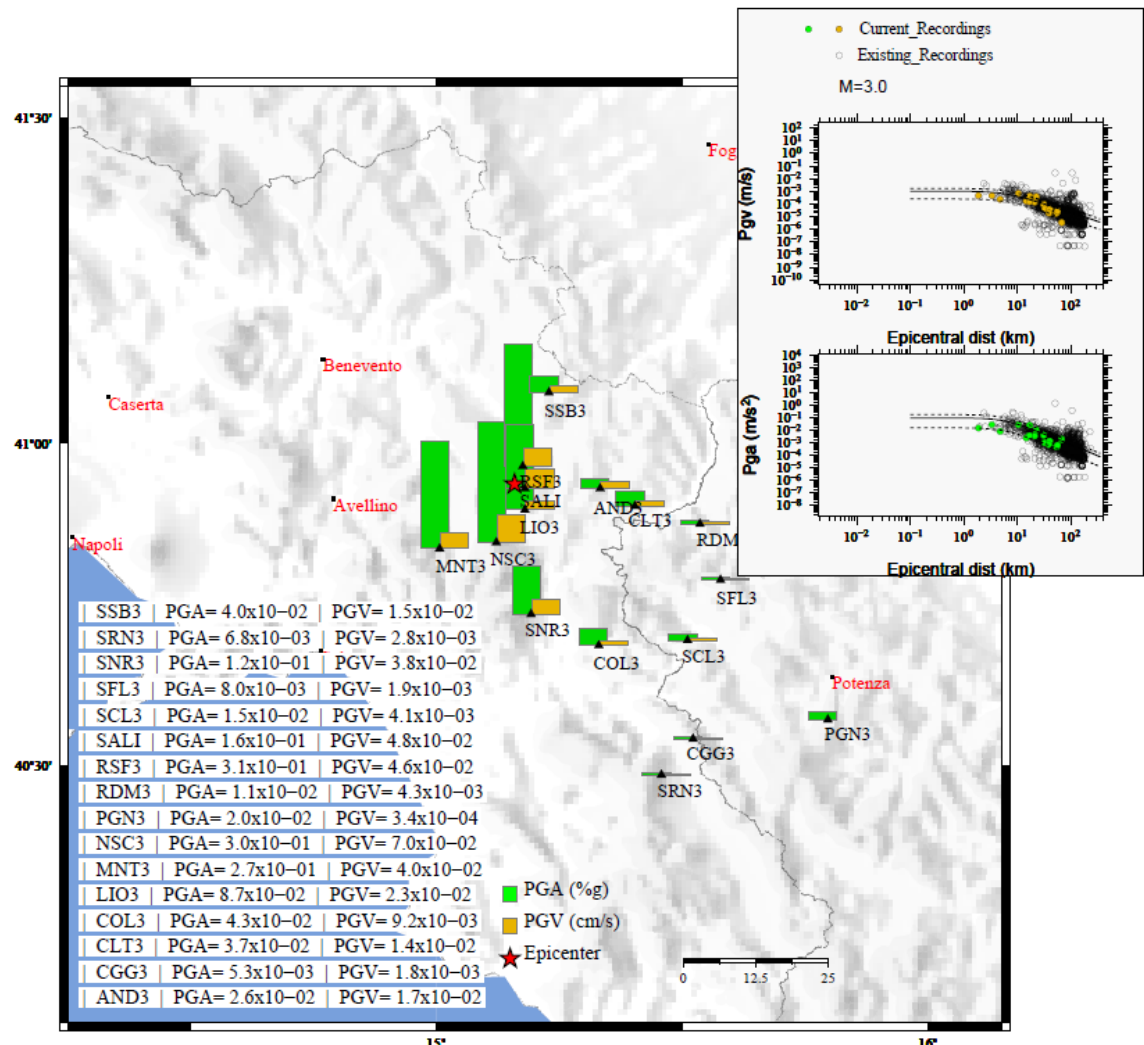


When analysing the ground motion for the other M 3.0 event (3/7/20 16:19), both PGA and Intensity maps computed with ShakeMap software **show maps elongated** along the NS direction, and a smaller amplitude than for the previous event of same magnitude.

PERCEIVED SHAKING	Not felt	Weak	Light	Moderate	Strong	Very strong	Severe	Violent	Extreme
POTENTIAL DAMAGE	none	none	none	Very light	Light	Moderate	Moderate/Heavy	Heavy	Very Heavy
PEAK ACC. (%g)	<.17	.17-1.4	1.4-3.8	3.8-8.2	8.2-18	18-34	34-85	85-124	>124
PEAK VEL. (cm/s)	<0.1	0.1-1.1	1.1-3.4	3.4-8.1	8.1-18	18-31	31-60	60-118	>118
INSTRUMENTAL INTENSITY	I	II-III	IV	V	VI	VII	VIII	IX	X+

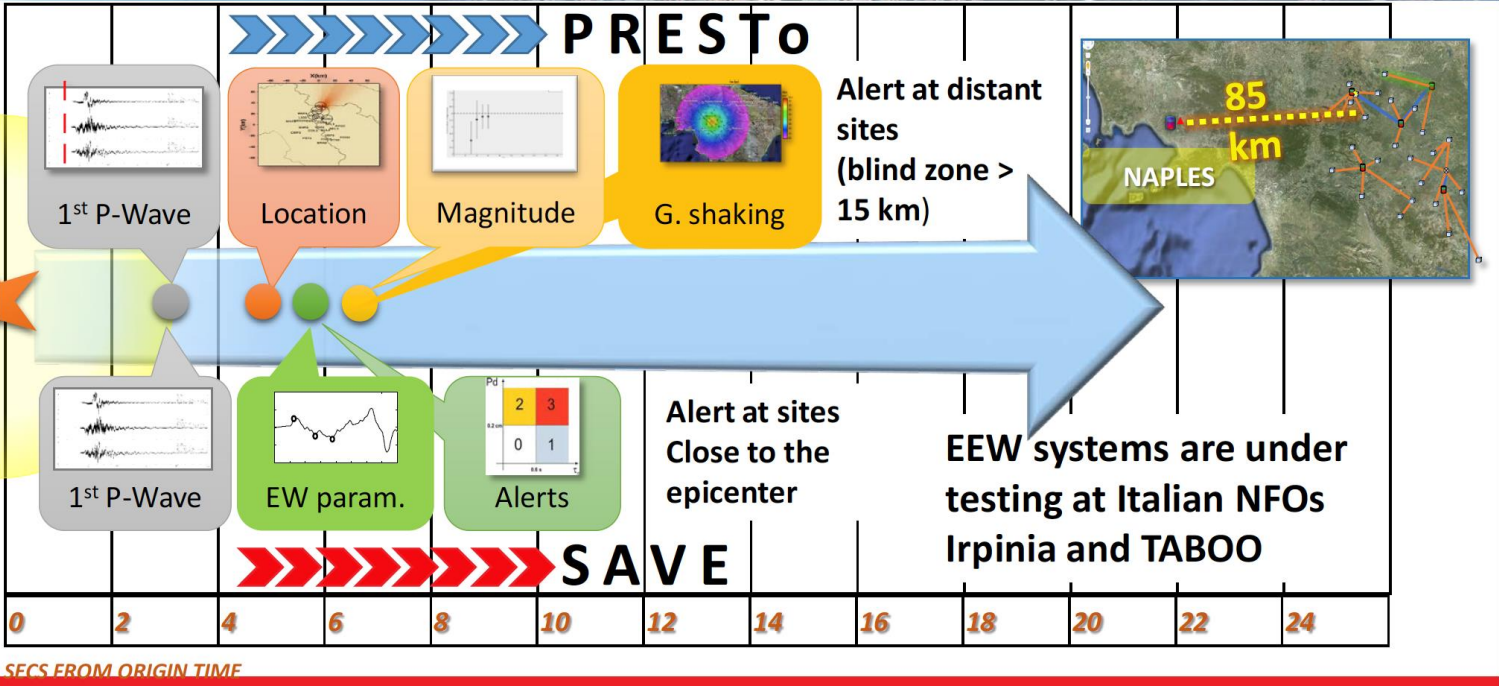
GMPE – M3.0

3/7/20 – 16:19



The amplitudes for this second event show a similar pattern than for the previous event, but **amplitudes are significantly smaller** mainly for lateral stations. This difference may be ascribed to the **diverse stress drop**: for the first event the stress drop is **6.1 MPa** while for the second event is **1.1 MPa**.

PRESTo and SAVE EEWS



Here we present the results for the **early warning systems** running in real-time on the Irpinia seismic network. In the regional system **PRESTo** (Satriano et al., 2010) the alert results from the analysis of signals recorded by a network of stations and the prompt estimation of location, magnitude and ground shaking prediction through specific GMPEs. In the onsite system **SAVE** (Caruso et al., 2017) the alert is obtained from a single station analysis and it is based on the direct estimation of the predicted intensity at the site as given by the measure of the first P-wave amplitude. The blind zone is the region within which the strong shaking waves arrive before the alert.

Overall performance of PRESTo

Event ID	ML	Mw	MPRESTo	DM_first
16975	1.4	2	1.5	0.1
16973	2.1	2.4	2.1	0
16972	2.1	2.3	2.5	0.4
16967	2.8	2.9	3.4	0.6
16964	2	2.3	2	0
16963	2.8	2.9	3	0.2
16962	1.9	2.2	1.9	0
16961	1.8	2.2	1.2	-0.6
16958	1.3	1.8	1.2	-0.1
16956	2.7	2.8	3.1	0.4

MAIN OUTCOMES:

@ FIRST Alert estimate:

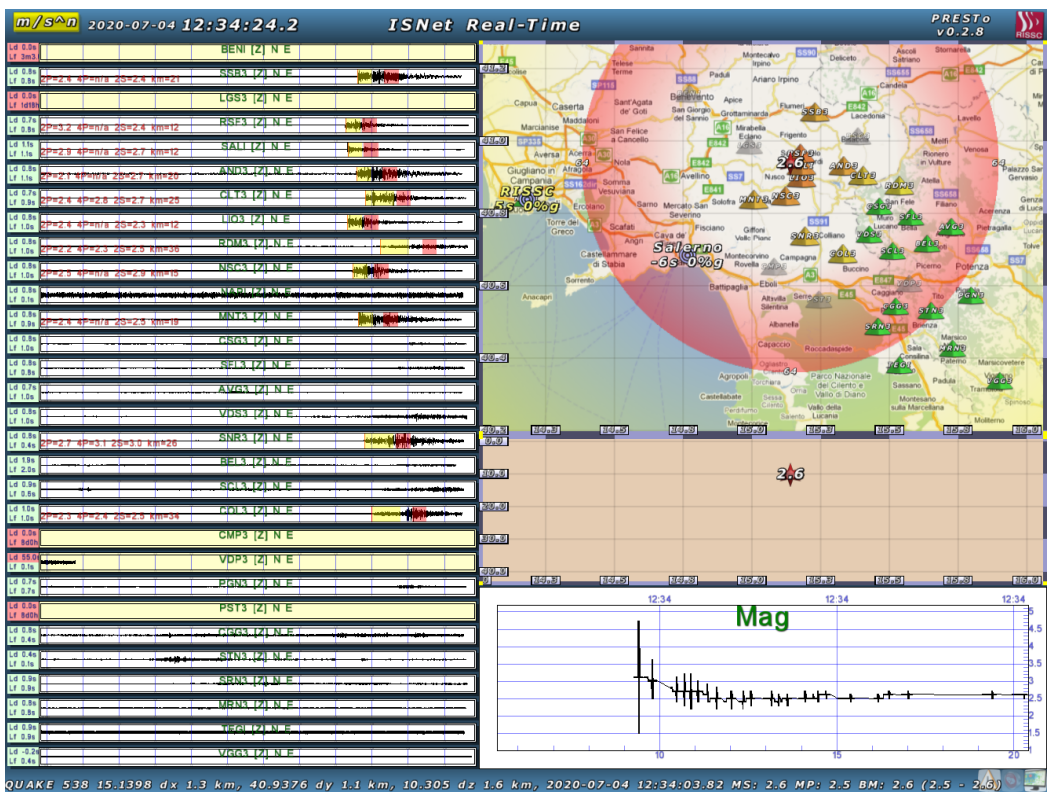
DeltaM: from 0 to 0.6

Average DeltaM = **0.26**

First Magnitude estimate on average available in **3.9s** from the first P-wave detection

The PRESTo EWS detected **10 events** of the sequence with M between 1.8 and 2.9; during the first day of the sequence, a temporary failure of the real-time communication prevented from a correct operation of the early warning system. For each event, the table shows the comparison between the local (M_L) and moment (M_w) magnitude (as computed by ISNet) and the estimated magnitude by PRESTo at the first alert. The difference between MPRESTo and M_L is also shown. We found that the first magnitude estimate is available on average **after 3.9s after the first P wave detection**.

Real-Time Performance of PRESTo for M2.7, 04-07 12:34 event



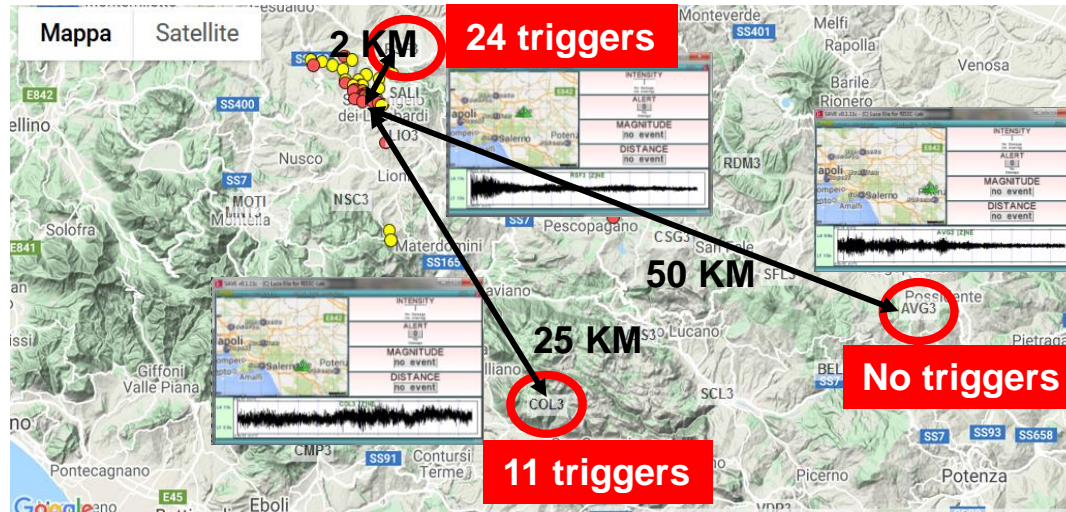
FIRST PRESTo estimate:
 6 sec after the origin time
 MAG error: +0.4
 LOC_epi error : 8 Km
 LOC_dep_error: 6 km

END of earthquake PRESTo estimate:
 18 sec after origin time
 MAG error : -0.1
 LOC_epi error : 1.21 Km
 LOC_dep_error: 1.8 km

DATA LATENCY:

- 23 stations with average data latency = 0.99 s
- 3 stations with latency > 30s (problems)
- 3 stations non available (problems)

SAVE during the M3.0, 07-03 16:14 event



- Three stations were operational during the sequence: RSF3, COL3 and AVG3, at different distances from the sequence hypocenters.
- We recovered 24 detection at the closest station RSF3, 11 alerts at COL3 and no alerts at AVG3.
- SAVE correctly predicted the expected ground motion intensity for all of the sites.
- SAVE was not able to measure the τ_c parameters, thus not providing any information about event magnitude.

ISNet_EWApp



The ISNet EWapp (Colombelli et al., 2020) currently being tested by 7 users in the RISSC lab, broadcast the alert related to 21 events of the sequence to the users smartphones, located in Naples, Avellino and Nocera Inferiore. For all the events, the intensity never overcame the threshold of intensity IV at the location of the smartphones.

References

- Adinolfi, G. M., Cesca, S., Picozzi, M., Heimann, S., & Zollo, A. (2019). Detection of weak seismic sequences based on arrival time coherence and empiric network detectability: an application at a near fault observatory. *Geophysical Journal International*, 218(3), 2054-2065.
- Amoroso, O., Ascione, A., Mazzoli, S., Virieux, J., & Zollo, A. (2014). Seismic imaging of a fluid storage in the actively extending Apennine mountain belt, southern Italy. *Geophysical Research Letters*, 41(11), 3802-3809.
- Ascione, A., Mazzoli, S., Petrosino, P., & Valente, E. (2013). A decoupled kinematic model for active normal faults: Insights from the 1980, MS= 6.9 Irpinia earthquake, southern Italy. *Bulletin*, 125(7-8), 1239-1259.
- Bergen K. J., & Beroza G. C. (2018). Detecting earthquakes over a seismic network using single-station similarity measures. *Geophys. J. Int.* 213, 1984-1998.
- Bernard, P., & Zollo, A. (1989). The Irpinia (Italy) 1980 earthquake: detailed analysis of a complex normal faulting. *Journal of Geophysical Research: Solid Earth*, 94(B2), 1631-1647.
- Bobbio A., Vassallo M., Festa G. A local magnitude scale for southern Italy, *Bulletin of of Seismological Society of America*, Vol. 99, No.4, 2461–2470, 2009 doi: 10.1785/0120080364
- Caruso, A., Colombelli, S., Elia, L., Picozzi, M., and Zollo, A. (2017), An on-site alert level early warning system for Italy, *J. Geophys. Res. Solid Earth*, 122, 2106– 2118, doi:10.1002/2016JB013403.
- Chiarabba, C., Jovane, L., & Di Stefano, R. (2005). A new view of Italian seismicity using 20 years of instrumental recordings. *Tectonophysics*, 395(3-4), 251-268.
- Cocco, M., Chiarabba, C., Di Bona, M., Selvaggi, G., Margheriti, L., Frepoli, A., ... & Campillo, M. (1999). The April 1996 Irpinia seismic sequence: evidence for fault interaction. *Journal of seismology*, 3(1), 105-117.
- Colombelli, S., A. Emolo and A. Zollo. A Duration Magnitude Scale for the Irpinia Seismic Network, *Southern Italy Seismological Research Letters*, January/February 2014, v. 85, p. 98-107, doi:10.1785/022013005
- Colombelli, S., Carotenuto, F., Elia, L., and Zollo, A.: Design and implementation of a mobile device app for network-based earthquake early warning systems (EEWSs): application to the PRESto EEWS in southern Italy, *Nat. Hazards Earth Syst. Sci.*, 20, 921–931, <https://doi.org/10.5194/nhess-20-921-2020>, 2020.
- De Landro, G., Amoroso, O., Stabile, T. A., Matrullo, E., Lomax, A., & Zollo, A. (2015). High-precision differential earthquake location in 3-D models: evidence for a rheological barrier controlling the microseismicity at the Irpinia fault zone in southern Apennines. *Geophysical Supplements to the Monthly Notices of the Royal Astronomical Society*, 203(3), 1821-1831.

References

- De Matteis, R., Matrullo, E., Rivera, L., Stabile, T. A., Pasquale, G., & Zollo, A. (2012). Fault delineation and regional stress direction from the analysis of background microseismicity in the southern Apennines, Italy. *Bulletin of the Seismological Society of America*, 102(4), 1899-1907
- DISS Working Group (2018). Database of Individual Seismogenic Sources (DISS), Version 3.2.1: A compilation of potential sources for earthquakes larger than M 5.5 in Italy and surrounding areas. <http://diss.rm.ingv.it/diss/>, Istituto Nazionale di Geofisica e Vulcanologia;
- Doglioni, C. (1995). Geological remarks on the relationships between extension and convergent geodynamic settings. *Tectonophysics*, 252(1-4), 253-267.
- Emolo, A., Convertito, V., & Cantore, L. (2011). Ground motion predictive equations for low-magnitude earthquakes in the Campania-Lucania area, Southern Italy. *J. geophys. Eng.* 8(1), 46-60.
- Iannaccone, G., Zollo, A., Elia, L., Convertito, V., Satriano, C., Martino, C., ... & Vassallo, M. (2010). A prototype system for earthquake early-warning and alert management in southern Italy. *Bulletin of Earthquake Engineering*, 8(5), 1105-1129.
- Improta, L., De Gori, P., & Chiarabba, C. (2014). New insights into crustal structure, Cenozoic magmatism, CO₂ degassing, and seismogenesis in the southern Apennines and Irpinia region from local earthquake tomography. *Journal of Geophysical Research: Solid Earth*, 119(11), 8283-8311.
- Lomax, A., Michelini, A., & Curtis, A. (2009). Earthquake location, direct, global-search methods. *Encyclopedia of complexity and systems science*, 5, 2449-2473.
- Malagnini L. and Munafò I., Short Note: On the Relationship between ML and Mw in a Broad Range: An Example from the Apennines, Italy. *Bulletin of the Seismological Society of America*, Vol. XX, No. XX, pp. –, – 2018, doi: 10.1785/0120170303
- Patacca, E., & Scandone, P. (2007a). Geology of the southern Apennines. *Bollettino della Società Geologica Italiana*, 7, 75-119.
- Picozzi, M., Bindi, D., Zollo, A. et al. Detecting long-lasting transients of earthquake activity on a fault system by monitoring apparent stress, ground motion and clustering. *Sci Rep* 9, 16268 (2019) doi:10.1038/s41598-019-52756-8
- Picozzi, M., Bindi, D., Spallarossa, D., Di Giacomo, D., Zollo A. (2018). A rapid response magnitude scale for timely assessment of the high frequency seismic radiation. *Scientific Reports – Nature* (2018) 8:8562 | DOI:10.1038/s41598-018-26938-9.
- Reasenber, P. A. (1985). FPFIT, FPLOT, and FPPAGE: Fortran computer programs for calculating and displaying earthquake fault-plane solutions. *US Geol. Surv. Open-File Rep.*, 85-739.
- Rovida A., Locati M., Camassi R., Lolli B., Gasperini P. (2019). Catalogo Parametrico dei Terremoti Italiani (CPTI15), versione 2.0. Istituto Nazionale di Geofisica e Vulcanologia (INGV). <https://doi.org/10.13127/CPTI/CPTI15.2>

References

- Claudio Satriano, Luca Elia, Claudio Martino, Maria Lancieri, Aldo Zollo, Giovanni Iannaccone. PRESTo, the earthquake early warning system for Southern Italy: Concepts, capabilities and future perspectives, *Soil Dynamics and Earthquake Engineering*, Volume 31, Issue 2, 2011, Pages 137-153, <https://doi.org/10.1016/j.soildyn.2010.06.008>.
- Supino, M., Festa, G., & Zollo, A. (2019). A probabilistic method for the estimation of earthquake source parameters from spectral inversion: application to the 2016–2017 Central Italy seismic sequence. *Geophysical Journal International*, 218(2), 988-1007.
- Yoon C. E., O'Reilly O., Bergen K. J., Beroza G. C. (2017). Earthquake detection through computationally efficient similarity search. *Science Advances*, 1, 11, e1501057.
- Zollo, A., Orefice, A., & Convertito, V. (2014). Source parameter scaling and radiation efficiency of microearthquakes along the Irpinia fault zone in southern Apennines, Italy. *Journal of Geophysical Research: Solid Earth*, 119(4), 3256-3275.



**RISSC-Lab: Laboratorio
di Ricerca in Sismologia
Sperimentale
e Computazionale**



**Irpinia Near-Fault
Observatory**



**Università degli studi
di Napoli Federico II**

Link utili:

ISNet <http://isnet.unina.it/>

ISNet Bulletin <http://isnet-bulletin.fisica.unina.it/cgi-bin/isnet-events/isnet.cgi>

RISSC-lab <http://www.rissclab.unina.it/>